Supporting Information for

Climate, demography, immunology, and virology combine to structure two decades of dengue dynamics in Cambodia

Cara E. Brook[1*], Carly Rozins[2], Jennifer A. Bohl[3], Vida Ahyong[4], Sophana Chea[5], Liz Fahsbender[6], Rekol Huy[7], Sreyngim Lay[5], Rithea Leang[7], Yimei Li[1], Chanthap Lon[5], Somnang Man[5,7], Mengheng Oum[5], Graham R. Northrup[8], Fabiano Oliveira[3], Andrea R. Pacheco[5], Daniel M. Parker[9], Katherine Young[10], Michael Boots[11], Cristina M. Tato[4], Joseph L. DeRisi[4], Christina Yek[3], Jessica E. Manning[3,5]

*Corresponding author: Cara E. Brook

Email: cbrook@uchicago.edu

This PDF file includes:

Supporting Information Text

Supporting Text 1: The TSIR Model

One of the simplest and most celebrated epidemic models, the Susceptible-Infectious-Recovered (SIR) model describes the dynamics of infectious disease transmission through a well-mixed host population, driven by rates of transmission (β) and recovery (γ) from infection, coupled with host demographic processes of birth (B) and death μ (1, 2). In its most standard form, the SIR model assumes that all individuals are born susceptible and that immunity after infection is lifelong:

$$\frac{dS}{dt} = B + \frac{\beta SI}{N} - \mu S$$
$$\frac{dI}{dt} = \frac{\beta SI}{N} - \gamma I - \mu I$$
$$\frac{dR}{dt} = \gamma I - \mu R$$

[1]

In standard annotation, the transmission rate (β) and the proportion of the population infected ($\frac{I}{N}$) can be characterized simply as the 'force of infection' (λ), the rate at which susceptibles become infected. One widely-used subclass of SIR models, the time series Susceptible-Infected-Recovered model, or the TSIR, was developed to simplify the process of parameter estimation in the fitting of SIR models to time series data, particularly for perfectly-immunizing childhood infections (e.g. measles) (3–6). The TSIR depends on two key assumptions: (*i*) that the pathogen infectious period is equal to the data sampling interval (classically, biweekly for measles) and (*ii*) that, over lengthy, 10-20 year time horizons, the sum of infected cases should roughly equal the sum of births for highly infectious childhood diseases for which all individuals are expected to eventually be exposed. The model assumes no overlapping generations of infection, and, following this logic, approximates the number of infections in a given timestep as the product of the susceptible population multiplied by the force of infection in the preceding timestep (equation [2]), where the homogeneity parameter (α) captures epidemic saturation and serves as a correction factor in the process of switching the model from continuous to discrete time:

$$S_{t+1} = B_t - S_t - I_t$$
$$I_{t+1} = \beta_{t+1} S_t I_t^{\alpha}$$

[2]

Given a time series of infected cases of childhood disease, the TSIR framework can thus be implemented by first reconstructing the susceptible population. In this process, a regression model is fitted between cumulative cases and cumulative births. If assumed to be equal, the slope of this regression model gives the reporting rate through time (ρ_t), and the residuals from this slope, (Z_t), represent heterogeneity in the susceptible population beyond the average. The mean of the susceptible population across the time series, ($\bar{S}$), can then be inferred from profile likelihood, and the time-varying regression rate (β_t), along with the homogeneity parameter (α) can be estimated using a generalized linear model after the following form:

$$\log I_{t+1} = \log \beta_{t+1} + \log(Z_t + \bar{S}) + \alpha \log I_t$$

[3]

A complete description of the TSIR model and underlying algorithms can be viewed in Finkenstädt and Grenfell 2000 (5). For the purposes of our analysis, we implemented the TSIR model using the R-package, tSIR, from Becker and Grenfell 2017 (3). Fixed and estimated parameter values for discrete fits to three subsets of dengue time series (2002-2006, 2008-2011, and 2013-2018) are available for viewing in Supplementary Table S2.

To implement a climate-informed TSIR model, we expressed the log of the biweekly transmission rate as a function of the optimally lagged biweekly mean temperature and total precipitation for the province and year in question. We investigated three forms of regression analyses by which to best represent the time-varying transmission rate, exploring a standard linear mixed effects regression; a linear mixed effects regression for the precipitation term, coupled with a Brière function for temperature; and a generalized addition model (GAM) (7), which we ultimately selected for the results reported in the main text.

The linear mixed effect regression (output visualized in Fig. S8A, S9A, S10A), took the following form:

$$\log \beta_{t,i} = \alpha_0 + B_1 T_{lag_{t,i}} + B_2 P_{lag_{t,i}} + \mu_{0,i} + \varepsilon_{t,i} \quad [4]$$

where $B_1$and B_2 represent the slopes of the fixed predictors (respectively, lagged temperature T_{lag} and lagged precipitation P_{lag}) for a specific province i at time t, $\mu_{0,i}$ is the province-specific random intercept, and $\varepsilon_{t,i}$ is a normally distributed error term.

Following (8), we also explored a combined linear mixed effects regression for lagged precipitation and a Brière function for lagged temperature, such that the temperature term in equation [4] was replaced with the following function:

$$f_{Brière} T_{lag_{t,i}} = c(T_{lag_{t,i}} - T_{min})(T_{max} - T_{lag_{t,i}})^{1/2} \quad [5]$$

Mirroring previous work (9), we embraced maximum flexibility in delineating the relationship between climate predictors and biweekly transmission using a GAM in which the time-varying climatological covariates were fit as smooth splines (Fig. S8C, S9C, S10C:

$$\log \beta_{t,i} = s\left[T_{lag_{t,i}}\right] + s\left[P_{lag_{t,i}}\right] + \mu_{0,i} + \varepsilon_{t,i} \quad [6]$$

where the s terms represent smoothing splines, $\mu_{0,i}$ is the province-specific random intercept, and $\varepsilon_{t,i}$ is a normally distributed error term. Because all models produced results that were qualitatively similar, and this last model offered maximal flexibility to capture subtle variation across provinces and timesteps, we selected this form to project epidemic year transmission rates for TSIR prediction.

Supporting Text 2: The FOI age-cumulative incidence model

Methods for estimating the force of infection (FOI, λ) from age-structured serological data for perfectly immunizing infections have been long-established and are well-described (7–9): these models demonstrate that the proportion of individuals seropositive in a given age class can be approximated by age-specific FOIs that accumulate across the duration of time spent within the corresponding age class—akin to a survival model under variable age-specific hazards of mortality. Estimation of age-structured seroprevalence is more complex for dengue, as a result of the dynamics of four co-circulating serotypes, for which infection results in longterm homotypic immunity but enhanced susceptibility to heterotypic serotypes. More recent work additionally suggests that secondary infections with homotypic serotypes may be possible following primary infections, provided sufficient phylogenetic distance between the genotypes responsible for primary and secondary infections (10).

2.1. Multi-typic exposures with life-long immunity

For lifelong immunizing childhood infections for which all individuals are expected to experience infection at some point in their lifetime, the hazard of exposure will compile cumulatively with increasing time since birth (e.g. with age), making time and age interchangeable units. As a result, data describing the age-distribution of exposures can be used to estimate the force of infection (as it varies with time or age or both) in a given system.

Ferguson et al. 1999 (11) present a system of equations (PDEs) describing the dynamics of a multitypic dengue infection with rates in terms of time, t, and age, a. Ferguson et al.1999 then derive equivalent expressions describing the time-and-age-dependent population of susceptibles (x), the time-and-age-dependent population of individuals exposed to only a primary infection with serotype i (z_i), and the time-and-age-dependent population of individuals experiencing any multitypic (2+ exposures) infection (z_m):

$$x(a,t) = e^{-\int_0^a \sum_i \lambda_i(a-\tau,t-\tau)d\tau} \quad [7]$$

$$z_i(a,t) = \left(e^{-\int_0^a \sum_{k\neq i} \lambda_k(a-\tau,t-\tau)d\tau}\right)\left(1 - e^{-\int_0^\infty \lambda_i(a-\tau,t-\tau)d\tau}\right) \quad [8]$$

$$z_m(a,t) = 1 - x(a,t) - \sum_i z_i(a,t) \quad [9]$$

In equation (7) – (9), the term τ reflects the inherent confounding between time t and age a. The two variables change at the same rate (i.e. $^{dt}/_{da} = 1$) and therefore once an individual is born, the difference between their age and the current "time" remains fixed and can be tracked with a single time dependent variable.

Equation [8] describes the population of individuals exposed to only a primary infection with serotype i (z_i) and can be read as the product of two probabilities:
(the probability of avoiding infection with all serotypes except for i, up to time t).
×(the probability of not avoiding infection with serotype i)

Using equation [7], this expression can also be rewritten as:

$$z_i(a,t) = x(a,t)\left[e^{\int_0^a \lambda_i(a-\tau,t-\tau)d\tau} - 1\right] \quad [10]$$

Following Cummings et al. 2009 (12), we first estimate a time-varying, annual FOI for our Cambodian dengue system, then later add in variation by age class shared across all years and provinces in the dataset.

Cummings et al. 2009 (12) discretized the Ferguson system shown above, creating a piece-wise solution whereby they estimate an annual mean FOI ($\bar{\lambda}$) representative for all serotypes (because the available data are not serotype-specific, serotype-specific FOIs, λ_i, cannot be distinguished). Following Cummings et al. 2009 (12), the integrand in equation [7] can be reformulated as:

$$\int_0^a \sum_i \lambda_i(a-\tau, t-\tau)d\tau = \sum_0^a N\bar{\lambda}\,(a-\tau, t-\tau)\Delta\tau \qquad [11]$$

where N corresponds to the number of circulating dengue serotypes in the system and $\Delta\tau$ corresponds to the duration of time acted on by each $\bar{\lambda}(a-\tau, t-\tau)$, here, for simplicity, always held constant at one year.

Following on above, the second integrand in equation 8 can also be reformulated as:

$$\int_0^a \lambda_i(a-\tau, t-\tau)d\tau = \sum_0^a \bar{\lambda}\,(a-\tau, t-\tau)\Delta\tau \qquad [12]$$

where, again, $\Delta\tau$ corresponds to the duration of time acted on by each $\bar{\lambda}(a-\tau, t-\tau)$, here held at one year.

We first followed Cummings et al. 2009 (12) to fit the above model to our dataset, estimating 40 distinct values for $\bar{\lambda}(t-\tau)$, one for each year from 1981-2020, beginning in the birth year (1981) of the oldest individual (22 years) in the first year (2002) of the dataset and extending through the last year of data for each province. Again, following Cummings et al. 2009 (12), we subsequently estimated 40 $\bar{\lambda}(t-\tau)$ paired with 26 age-specific variations on the annual $\bar{\lambda}(t-\tau)$, 13 of which were shared across all provinces and years up to 2010 and 13 of which were shared across all provinces and years after 2010.

2.2. Multitypic exposures with waning immunity

Because we observed a sharp increase in the number of dengue cases reported in older (50+ years) individuals in the later years of our dataset, we next extended the model presented in Ferguson et al. 1999 (11) to include a rate of waning multitypic immunity, which allowed for re-infection with the same serotype (i) in later age classes.

We can conceptualize our new system in the following box model:

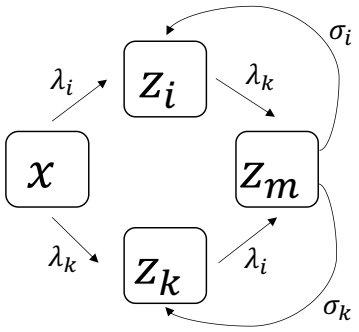

The above diagram assumes two circulating serotypes (represented with subscripts i and k , keeping with Ferguson's notation). Additional states could be added if additional serotypes were at play. Then we would use Ferguson's exact notation where i refers to the focal strain and $k \neq i$ is an index representing all of the other strains. Here, σ_i and σ_k represent waning from a multitypic exposure state back to a homotypic exposure state, allowing for re-exposure to z_m and presentation as a reported case. For simplicity, we assume these rates to be constant across age and time. With the exception of the σ terms, this model is identical to that presented in Ferguson et al. 1999 (11).

We express the first two terms in our system of differential equations as:

$$\frac{dx(a,t)}{dt} = -x \sum_i \lambda_i(a, t-a) \quad [13]$$

$$\frac{dz_i(a,t)}{dt} = x \sum_i \lambda_i(a, t-a) - \sum_{k \neq i} \lambda_k(a,t) + \sigma_i z_m(a,t) \quad [14]$$

where $z_i(a,t)$ represents the proportion of individuals that demonstrate history of homotypic infection with single strain i.

From [13], we can then solve directly for $x(a,t)$:

$$x(a,t) = Ce^{-\int_0^a \sum_j \lambda_j(a-\tau, t-\tau)d\tau} \quad [15]$$

where $j \in \{i,k\}$. We can then solve for C (the integration constant) under the assumption that the entire population is born susceptible, $x(0) = 1$. From this, we determine that $C = 1$, revealing that the susceptible population is represented by the same expression previously shown for the system without waning immunity in equation 7 above:

$$x(a,t) = e^{-\int_0^a \sum_j \lambda_j(a-\tau, t-\tau)d\tau} \quad [16]$$

Following Cummings et al. 2009 (12) and using Cambodia data which lack serotype-specific specifications, we can estimate the mean FOI per serotype, assuming N circulating serotypes in our system:

$$x(a,t) = e^{-\int_0^a N\bar{\lambda}(a-\tau, t-\tau)d\tau} \quad [17]$$

Following Ferguson, we can now derive an expression for $z_i(a,t)$. This expression should sum the probabilities of the two disparate routes by which an individual can enter this class, as highlighted in the diagram below—either progressing directly from x to z_i (black) or achieving z_m and then waning back into z_i (blue):

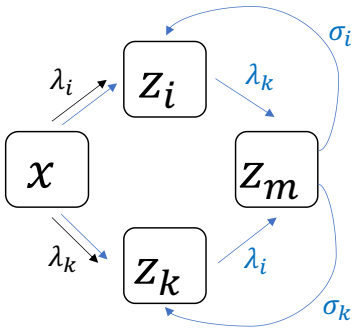

We write this new expression as the summed probabilities of the two pathways, with the second pathway described as the product of the sequential probabilities of each of the three steps taken:

$$z_i(a,t) = \left(e^{-\int_0^a \Sigma_{k\neq i}\lambda_k(a-\tau,t-\tau)d\tau}\right)\left(1-e^{-\int_0^\infty \lambda_i(a-\tau,t-\tau)d\tau}\right) + \left(e^{-\int_0^a \Sigma_{k\neq i}\lambda_k(a-\tau,t-\tau)d\tau}\right)\left(1-e^{-\int_0^\infty \lambda_i(a-\tau,t-\tau)d\tau}\right)\left(1-e^{-\int_0^\infty \Sigma_{k\neq i}\lambda_k(a-\tau,t-\tau)d\tau}\right)\left(e^{-\int_0^\infty \Sigma_{k\neq i}\sigma_k d\tau}\right)\left(1-e^{-\int_0^\infty \sigma_i d\tau}\right) \quad [18]$$

The summation term included with σ_k allows for the possibility of including greater than two serotypes by which an individual could wane out of the multitypic exposure state.

After Cummings et al. 2009 (12), we can again discretize the system and estimate the average rate of waning immunity across all serotypes, $\bar{\sigma}$. To this end, we can rewrite the last two integrands in equation [18] as:

$$\int_0^a \sum_{k\neq i} \sigma_k d\tau = (N-1)\bar{\sigma}\Delta\tau \quad [19]$$

$$\int_0^a \sigma_i d\tau = \bar{\sigma}\Delta\tau \quad [20]$$

where, again, $\Delta\tau$ corresponds to the duration of time acted on by $\bar{\sigma}$.

2.3. Fitting FOI models to the data

All versions of the above models (with and without age modification and/or waning multitypic immunity) were fit to the age distribution of cases per year, for each province and the national dataset as a whole using a quasi-Newton (L-BFGS-B) optimization method in the R package 'optim'. The fits of each model to the data were compared via AIC following convergence (Table S8). 95% confidence intervals were constructed from the hessian matrix for fits of the FOI and waning heterotypic immunity and by profiling the likelihood for the age modification terms.

Supporting Text 3: The structured, discrete-time epidemic model

To formalize our mechanistic hypotheses of the transmission dynamics underlying the patterns of elevated mean age of dengue infection and expansion of the age distribution of cases witnessed in our data, we developed an age-structured, discrete time, epidemic matrix model to allow us to simulate each hypothetical scenario (13–15).

Under this modeling approach, we can express the population as a vector $\boldsymbol{n}(t)$, divided into both age and epidemic classes. To model the dynamics of three circulating dengue serotypes, we allow for 35 discrete epidemic states and 100 annual age classes. Epidemic states take the following form:

- Susceptible to all serotypes (one state): S
- Primary infections (three states): I_1, I_2, I_3
- Recovered from primary infection and protected from reinfection with any serotype by heterotypic immunity (three states): P_1, P_2, P_3
- Protected by monotypic immunity from primary infection but susceptible to other serotypes due to waned heterotypic immunity (three states; here, subscript corresponds to the serotype to which the class is no longer susceptible): S_1, S_2, S_3
- Secondary infections (six states): $I_{12}, I_{13}, I_{21}, I_{23}, I_{31}, I_{32}$
- Recovered from secondary infection and protected from reinfection with any serotype by heterotypic immunity (six states): $P_{12}, P_{13}, P_{21}, P_{23}, P_{31}, P_{32}$
- Protected by multitypic immunity from secondary infection but susceptible to one other serotype due to waned heterotypic immunity (six states; here, subscript corresponds to the serotypes to which the class is no longer susceptible): $S_{12}, S_{13}, S_{21}, S_{23}, S_{31}, S_{32}$
- Tertiary infections (six states): $I_{123}, I_{132}, I_{213}, I_{231}, I_{312}, I_{321}$
- Finally, for simplicity, individuals who have experienced tertiary infection progress immediately to a state of multitypic immunity (one state): P_m

From above, the population vector takes the following form:

$$\boldsymbol{n}(t) = \left(S_{1,t,} \dots S_{a_{max},t}, I_{1_{1,t}} \dots I_{1_{a_{max},t}}, I_{2_{1,t}} \dots I_{2_{a_{max},t}}, \dots \dots \dots \dots \dots \dots \dots \dots \dots \; P_{m_{1,t}} \dots P_{m_{a_{max},t}}\right)$$

where a_{max} indicates the oldest age class in the model (here, 100 years).

Next, we investigated epidemic and demographic transitions for this population using a transition matrix. Following (15), we initially ignore demographic transitions (survival and aging), to describe transitions between the above 35 epidemic states within a single age class a according to:

$$\begin{bmatrix}
1-3(\bar{\lambda}) & 0 & 0 & 0 & 0 & 0 & 0 & 0 & 0 & 0 & 0 & 0 & 0 & 0 & 0 & 0 & 0 & 0 & 0 & 0 & 0 & 0 & 0 & 0 & 0 & 0 & 0 & 0 & 0 & 0 & 0 & 0 & 0 & 0 & 0 & 0 & 0 \\
\bar{\lambda} & 1-r & 0 & 0 & 0 & 0 & 0 & 0 & 0 & 0 & 0 & 0 & 0 & 0 & 0 & 0 & 0 & 0 & 0 & 0 & 0 & 0 & 0 & 0 & 0 & 0 & 0 & 0 & 0 & 0 & 0 & 0 & 0 & 0 & 0 & 0 & 0 \\
\bar{\lambda} & 0 & 1-r & 0 & 0 & 0 & 0 & 0 & 0 & 0 & 0 & 0 & 0 & 0 & 0 & 0 & 0 & 0 & 0 & 0 & 0 & 0 & 0 & 0 & 0 & 0 & 0 & 0 & 0 & 0 & 0 & 0 & 0 & 0 & 0 & 0 & 0 \\
\bar{\lambda} & 0 & 0 & 1-r & 0 & 0 & 0 & 0 & 0 & 0 & 0 & 0 & 0 & 0 & 0 & 0 & 0 & 0 & 0 & 0 & 0 & 0 & 0 & 0 & 0 & 0 & 0 & 0 & 0 & 0 & 0 & 0 & 0 & 0 & 0 & 0 & 0 \\
0 & r & 0 & 0 & 1-\omega & 0 & 0 & 0 & 0 & 0 & 0 & 0 & 0 & 0 & 0 & 0 & 0 & 0 & 0 & 0 & 0 & 0 & 0 & 0 & 0 & 0 & 0 & 0 & 0 & 0 & 0 & 0 & 0 & 0 & 0 & 0 & 0 \\
0 & 0 & r & 0 & 0 & 1-\omega & 0 & 0 & 0 & 0 & 0 & 0 & 0 & 0 & 0 & 0 & 0 & 0 & 0 & 0 & 0 & 0 & 0 & 0 & 0 & 0 & 0 & 0 & 0 & 0 & 0 & 0 & 0 & 0 & 0 & 0 & 0 \\
0 & 0 & 0 & r & 0 & 0 & 1-\omega & 1-2(\bar{\lambda}) & 0 & 0 & 0 & 0 & 0 & 0 & 0 & 0 & 0 & 0 & 0 & 0 & 0 & 0 & 0 & 0 & 0 & 0 & 0 & 0 & 0 & 0 & 0 & 0 & 0 & 0 & 0 & 0 & \sigma \\
0 & 0 & 0 & 0 & \omega & 0 & 0 & 0 & 1-2(\bar{\lambda}) & 0 & 0 & 0 & 0 & 0 & 0 & 0 & 0 & 0 & 0 & 0 & 0 & 0 & 0 & 0 & 0 & 0 & 0 & 0 & 0 & 0 & 0 & 0 & 0 & 0 & 0 & 0 & \sigma \\
0 & 0 & 0 & 0 & 0 & \omega & 0 & 0 & 0 & 1-2(\bar{\lambda}) & 0 & 0 & 0 & 0 & 0 & 0 & 0 & 0 & 0 & 0 & 0 & 0 & 0 & 0 & 0 & 0 & 0 & 0 & 0 & 0 & 0 & 0 & 0 & 0 & 0 & 0 & \sigma \\
0 & 0 & 0 & 0 & 0 & 0 & \omega & 0 & 0 & 0 & 1-2(\bar{\lambda}) & 0 & 0 & 0 & 0 & 0 & 0 & 0 & 0 & 0 & 0 & 0 & 0 & 0 & 0 & 0 & 0 & 0 & 0 & 0 & 0 & 0 & 0 & 0 & 0 & 0 & \sigma \\
0 & 0 & 0 & 0 & 0 & 0 & 0 & \bar{\lambda} & 0 & 0 & 0 & 1-r & 0 & 0 & 0 & 0 & 0 & 0 & 0 & 0 & 0 & 0 & 0 & 0 & 0 & 0 & 0 & 0 & 0 & 0 & 0 & 0 & 0 & 0 & 0 & 0 & 0 \\
0 & 0 & 0 & 0 & 0 & 0 & 0 & \bar{\lambda} & \bar{\lambda} & 0 & 0 & 0 & 1-r & 0 & 0 & 0 & 0 & 0 & 0 & 0 & 0 & 0 & 0 & 0 & 0 & 0 & 0 & 0 & 0 & 0 & 0 & 0 & 0 & 0 & 0 & 0 & 0 \\
0 & 0 & 0 & 0 & 0 & 0 & 0 & \bar{\lambda} & \bar{\lambda} & 0 & 0 & 1-r & 0 & 0 & 0 & 0 & 0 & 0 & 0 & 0 & 0 & 0 & 0 & 0 & 0 & 0 & 0 & 0 & 0 & 0 & 0 & 0 & 0 & 0 & 0 & 0 & 0 \\
0 & 0 & 0 & 0 & 0 & 0 & 0 & 0 & \bar{\lambda} & 0 & 0 & 0 & 1-r & 0 & 0 & 0 & 0 & 0 & 0 & 0 & 0 & 0 & 0 & 0 & 0 & 0 & 0 & 0 & 0 & 0 & 0 & 0 & 0 & 0 & 0 & 0 & 0 \\
0 & 0 & 0 & 0 & 0 & 0 & 0 & 0 & 0 & 0 & 0 & 0 & 0 & 1-r & 0 & 0 & 0 & 0 & 0 & 0 & 0 & 0 & 0 & 0 & 0 & 0 & 0 & 0 & 0 & 0 & 0 & 0 & 0 & 0 & 0 & 0 & 0 \\
0 & 0 & 0 & 0 & 0 & 0 & 0 & 0 & 0 & 0 & 0 & 0 & 0 & 0 & 1-r & 0 & 0 & 0 & 0 & 0 & 0 & 0 & 0 & 0 & 0 & 0 & 0 & 0 & 0 & 0 & 0 & 0 & 0 & 0 & 0 & 0 & 0 \\
0 & 0 & 0 & 0 & 0 & 0 & 0 & 0 & 0 & 0 & 0 & 0 & 0 & 0 & 0 & 1-\omega & 0 & 0 & 0 & 0 & 0 & 0 & 0 & 0 & 0 & 0 & 0 & 0 & 0 & 0 & 0 & 0 & 0 & 0 & 0 & 0 & 0 \\
0 & 0 & 0 & 0 & 0 & 0 & 0 & 0 & 0 & 0 & 0 & 0 & 0 & 0 & 0 & 0 & 1-\omega & 0 & 0 & 0 & 0 & 0 & 0 & 0 & 0 & 0 & 0 & 0 & 0 & 0 & 0 & 0 & 0 & 0 & 0 & 0 & 0 \\
0 & 0 & 0 & 0 & 0 & 0 & 0 & 0 & 0 & 0 & 0 & 0 & 0 & 0 & 0 & 0 & 0 & r & 0 & 0 & 0 & 0 & 0 & 0 & 0 & 0 & 0 & 0 & 0 & 0 & 0 & 0 & 0 & 0 & 0 & 0 & 0 \\
0 & 0 & 0 & 0 & 0 & 0 & 0 & 0 & 0 & 0 & 0 & 0 & 0 & 0 & 0 & 0 & 0 & 0 & r & 0 & 0 & 0 & 0 & 0 & 0 & 0 & 0 & 0 & 0 & 0 & 0 & 0 & 0 & 0 & 0 & 0 & 0 \\
0 & 0 & 0 & 0 & 0 & 0 & 0 & 0 & 0 & 0 & 0 & 0 & 0 & 0 & 0 & 0 & 0 & 0 & 0 & r & 0 & 0 & 0 & 0 & 0 & 0 & 0 & 0 & 0 & 0 & 0 & 0 & 0 & 0 & 0 & 0 & 0 \\
0 & 0 & 0 & 0 & 0 & 0 & 0 & 0 & 0 & 0 & 0 & 0 & 0 & 0 & 0 & 0 & 0 & 0 & 0 & 0 & r & 0 & 0 & 0 & 0 & 0 & 0 & 0 & 0 & 0 & 0 & 0 & 0 & 0 & 0 & 0 & 0 \\
0 & 0 & 0 & 0 & 0 & 0 & 0 & 0 & 0 & 0 & 0 & 0 & 0 & 0 & 0 & 0 & 0 & 0 & 0 & 0 & 0 & r & 0 & 0 & 0 & 0 & 0 & 0 & 0 & 0 & 0 & 0 & 0 & 0 & 0 & 0 & 0 \\
0 & 0 & 0 & 0 & 0 & 0 & 0 & 0 & 0 & 0 & 0 & 0 & 0 & 0 & 0 & 0 & 0 & 0 & 0 & 0 & 0 & 0 & r & 0 & 0 & 0 & 0 & 0 & 0 & 0 & 0 & 0 & 0 & 0 & 0 & 0 & 0 \\
0 & 0 & 0 & 0 & 0 & 0 & 0 & 0 & 0 & 0 & 0 & 0 & 0 & 0 & 0 & 0 & 0 & 0 & 0 & 0 & 0 & 0 & 0 & r & 0 & 0 & 0 & 0 & 0 & 0 & 0 & 0 & 0 & 0 & 0 & 0 & 0 \\
0 & 0 & 0 & 0 & 0 & 0 & 0 & 0 & 0 & 0 & 0 & 0 & 0 & 0 & 0 & 0 & 0 & 0 & 0 & 0 & 0 & 0 & 0 & 0 & r & 0 & 0 & 0 & 0 & 0 & 0 & 0 & 0 & 0 & 0 & 0 & 0 \\
0 & 0 & 0 & 0 & 0 & 0 & 0 & 0 & 0 & 0 & 0 & 0 & 0 & 0 & 0 & 0 & 0 & 0 & 0 & 0 & 0 & 0 & 0 & 0 & 0 & r & 0 & 0 & 0 & 0 & 0 & 0 & 0 & 0 & 0 & 0 & 0 \\
0 & 0 & 0 & 0 & 0 & 0 & 0 & 0 & 0 & 0 & 0 & 0 & 0 & 0 & 0 & 0 & 0 & 0 & 0 & 0 & 0 & 0 & 0 & 0 & 0 & 0 & r & 0 & 0 & 0 & 0 & 0 & 0 & 0 & 0 & 0 & 0 \\
0 & 0 & 0 & 0 & 0 & 0 & 0 & 0 & 0 & 0 & 0 & 0 & 0 & 0 & 0 & 0 & 0 & 0 & 0 & 0 & 0 & 0 & 0 & 0 & 0 & 0 & 0 & r & 0 & 0 & 0 & 0 & 0 & 0 & 0 & 0 & 0 \\
0 & 0 & 0 & 0 & 0 & 0 & 0 & 0 & 0 & 0 & 0 & 0 & 0 & 0 & 0 & 0 & 0 & 0 & 0 & 0 & 0 & 0 & 0 & 0 & 0 & 0 & 0 & 0 & r & 0 & 0 & 0 & 0 & 0 & 0 & 0 & 0 \\
0 & 0 & 0 & 0 & 0 & 0 & 0 & 0 & 0 & 0 & 0 & 0 & 0 & 0 & 0 & 0 & 0 & 0 & 0 & 0 & 0 & 0 & 0 & 0 & 0 & 0 & 0 & 0 & 0 & r & 0 & 0 & 0 & 0 & 0 & 0 & 0 \\
0 & 0 & 0 & 0 & 0 & 0 & 0 & 0 & 0 & 0 & 0 & 0 & 0 & 0 & 0 & 0 & 0 & 0 & 0 & 0 & 0 & 0 & 0 & 0 & 0 & 0 & 0 & 0 & 0 & 0 & r & 0 & 0 & 0 & 0 & 0 & 0 \\
0 & 0 & 0 & 0 & 0 & 0 & 0 & 0 & 0 & 0 & 0 & 0 & 0 & 0 & 0 & 0 & 0 & 0 & 0 & 0 & 0 & 0 & 0 & 0 & 0 & 0 & 0 & 0 & 0 & 0 & 0 & r & 0 & 0 & 0 & 0 & 0 \\
0 & 0 & 0 & 0 & 0 & 0 & 0 & 0 & 0 & 0 & 0 & 0 & 0 & 0 & 0 & 0 & 0 & 0 & 0 & 0 & 0 & 0 & 0 & 0 & 0 & 0 & 0 & 0 & 0 & 0 & 0 & 0 & r & 0 & 0 & 0 & 0 \\
0 & 0 & 0 & 0 & 0 & 0 & 0 & 0 & 0 & 0 & 0 & 0 & 0 & 0 & 0 & 0 & 0 & 0 & 0 & 0 & 0 & 0 & 0 & 0 & 0 & 0 & 0 & 0 & 0 & 0 & 0 & 0 & 0 & r & 0 & 0 & 0 \\
0 & 0 & 0 & 0 & 0 & 0 & 0 & 0 & 0 & 0 & 0 & 0 & 0 & 0 & 0 & 0 & 0 & 0 & 0 & 0 & 0 & 0 & 0 & 0 & 0 & 0 & 0 & 0 & 0 & 0 & 0 & 0 & 0 & 0 & r & 0 & 0 \\
0 & 0 & 0 & 0 & 0 & 0 & 0 & 0 & 0 & 0 & 0 & 0 & 0 & 0 & 0 & 0 & 0 & 0 & 0 & 0 & 0 & 0 & 0 & 0 & 0 & 0 & 0 & 0 & 0 & 0 & 0 & 0 & 0 & 0 & 0 & r & 0 \\
0 & 0 & 0 & 0 & 0 & 0 & 0 & 0 & 0 & 0 & 0 & 0 & 0 & 0 & 0 & 0 & 0 & 0 & 0 & 0 & 0 & 0 & 0 & 0 & 0 & 0 & 0 & 0 & 0 & 0 & 0 & 0 & 0 & 0 & 0 & 0 & r \\
0 & 0 & 0 & 0 & 0 & 0 & 0 & 0 & 0 & 0 & 0 & 0 & 0 & 0 & 0 & 0 & 0 & 0 & 0 & 0 & 0 & 0 & 0 & 0 & 0 & 0 & 0 & 0 & 0 & 0 & 0 & 0 & 0 & 0 & 0 & 0 & 1-3(\sigma)
\end{bmatrix}$$

[20]

where $\bar{\lambda}$ corresponds to the mean probability of transmission for a single serotype, r is the probability of recovery (equal to 1 if the model is simulated in biweekly timesteps according to the generation time of dengue), ω is the probability of waning heterotypic immunity, and σ is the probability of waning multitypic immunity, as described in the main text.

The above transition matrix describes the epidemic transitions assuming three endemic circulating serotypes in the system. This matrix can be modified to account for only two strains (e.g. some of the $\bar{\lambda}$ values become 0 and expressions of $1-3(\bar{\lambda})$ become $1-2(\bar{\lambda})$ instead) or to account for differing dynamical assumptions (e.g. whether waning multytypic immunity is considered).

From above, again following (15), we next add in demography, to construct the full transition matrix $\boldsymbol{A}(\boldsymbol{n}(t))$, which we use to project the entire population forwards (via aging, mortality and epidemic transitions) according to:

$$\boldsymbol{A}(\boldsymbol{n}(t)) = \begin{pmatrix} s_1(1-u_1)\boldsymbol{A}_1 & 0 & 0 & 0 & 0 & 0 \\ s_1u_1\boldsymbol{A}_1 & s_2(1-u_2)\boldsymbol{A}_2 & 0 & 0 & 0 & 0 \\ 0 & s_2u_2\boldsymbol{A}_2 & s_3(1-u_3)\boldsymbol{A}_3 & 0 & 0 & 0 \\ 0 & 0 & s_3u_3\boldsymbol{A}_3 & 0 & 0 & 0 \\ \ldots & \ldots & \ldots & \ldots & \ldots & 0 \\ 0 & 0 & 0 & 0 & 0 & .s_z\boldsymbol{A}_z \end{pmatrix}$$

[21]

where s_a is the probability that an individual of age class a survives to the next timestep, u_a is the probability of aging out of age class a and $\boldsymbol{A}_1$, $\boldsymbol{A}_2$, etc. correspond to the epidemic transition matrix in equation [20].

We then project the dynamics of the population as a whole forward by multiplying the population vector by the transition matrix and adding in a vector of annual births:

$$\boldsymbol{n}(t+1) = \boldsymbol{A}(\boldsymbol{n}(t))\boldsymbol{n}(t) + \boldsymbol{B}(t)$$

[22]

where $\boldsymbol{B}(t)$ is a vector of the number of births at time t:

$$\boldsymbol{B}(t) = (\boldsymbol{B}(t), 0, 0, \ldots 0)^T$$

[23]

From above, we simulated the dynamics of the five hypotheses outlined in the main text (H0: standard demography; H1: elevated FOI in epidemic years; H2: novel genotype invasion with waning immunity within the serotype; H3: novel serotype invasion; H4: 3 circulating serotypes with increasing tertiary case detection), tracking infection status per age category through time.

We simulated in biweekly timesteps, according to the generation time of the pathogen. We initiated our simulations with an initial population vector at t=0 using the proportional age distribution of the Cambodia from 1950, as recovered from (16) and 5 infected individuals in the first age class for each serotype under circulation. We first simulated dynamics out to equilibrium for 40 years, then, in the last 22 years of the time series, we introduced parameters that aimed to approximate the real-world dynamics of dengue in Cambodia over the past two decades.

Parameters were fixed at the following rates, which we converted to biweek probabilities prior to input into the transition matrix in equation [20]:

- $\bar{\lambda}$, the single-serotype FOI, was fixed at values estimated at the national level via the fitting of Ferguson-Cummings catalytic model in Fig. 3, from 1999-2020.

    - $\bar{\lambda}$ was further modified according to parameters estimated in Fig. 3 analyses.
    - We additionally introduced intra-annual climate variation to the FOI, by averaging biweekly transmission rates as estimated for TSIR across all provinces and years and rescaling them from 0.5 to 1.5 to allow for subtle seasonal dampening or amplification of the FOI.
- Births ($\boldsymbol{B}(t)$), were input annually outside of the transition matrix as shown in equation [22], corresponding to publicly available birth rates through time reported by the World Bank (17).
- Age-specific death rates (from which we calculated biweekly survival rates per age class) were obtained from the United Nations databank (18).
- Infected individuals were assumed to recover from infection in a single biweekly timestep (rate r).
- Heterotypic immunity was assumed to wane (ω) at a rate of $\frac{1}{2}$ yrs^{-1}, as estimated in the literature (19).
- Homotypic immunity was allowed to wane at rate (σ) in certain simulations, corresponding to estimates from fitting of extended FOI models in Fig. 3 analyses.

Antibody-dependent enhancement was not considered in this model.

After simulations of hypotheses were complete, we finally fit our Ferguson-Cummings catalytic model from Fig. 3 to the resulting distribution of cases by age, by year, to attempt to recover the input FOI across the time series. We additionally fit a parameter of waning immunity (σ) to each simulated dataset after estimating and fixing FOI, to evaluate the conditions under which this model was improved by consideration of waning immunity.

All code and corresponding data needed to reproduce all analyses and run all simulations can be viewed in our publicly available GitHub repository at: https://github.com/brooklabteam/cambodia-dengue-national

Supplementary Figures

Figure S1. Annual biweekly mean temperatures (^{0}C) for Cambodia, aggregated by province and year.

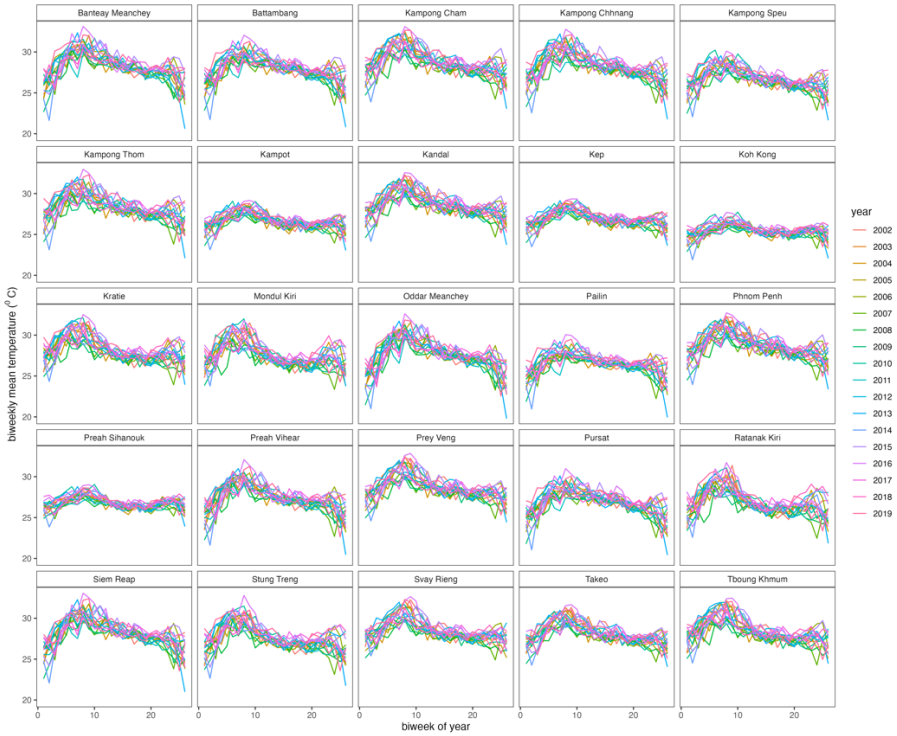

Figure S2. Annual biweekly total precipitation (mm) for Cambodia, aggregated by province and year.

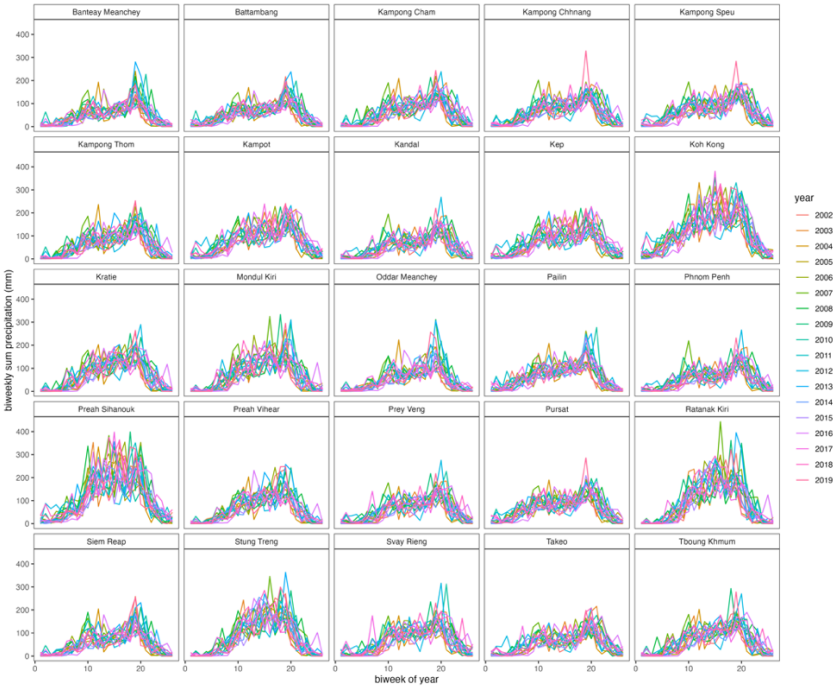

Figure S3. Interannual trends in mean biweekly temperature (^{0}C) for Cambodia, aggregated by province. Black lines give GAM predictions of interannual trends, with 95% confidence intervals by standard error shown as narrow shading around mean projection (Table S1).

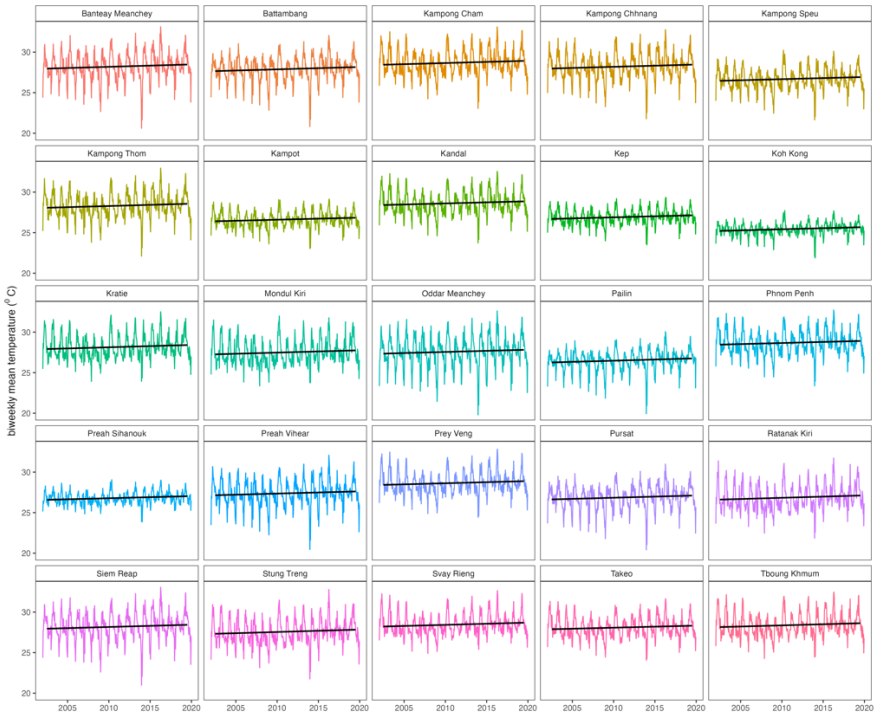

Figure S4. Interannual trends in total mean precipitation (mm) for Cambodia, aggregated by province. Black lines give GAM predictions of interannual trends, with 95% confidence intervals by standard error shown as narrow shading around mean projection (Table S1).

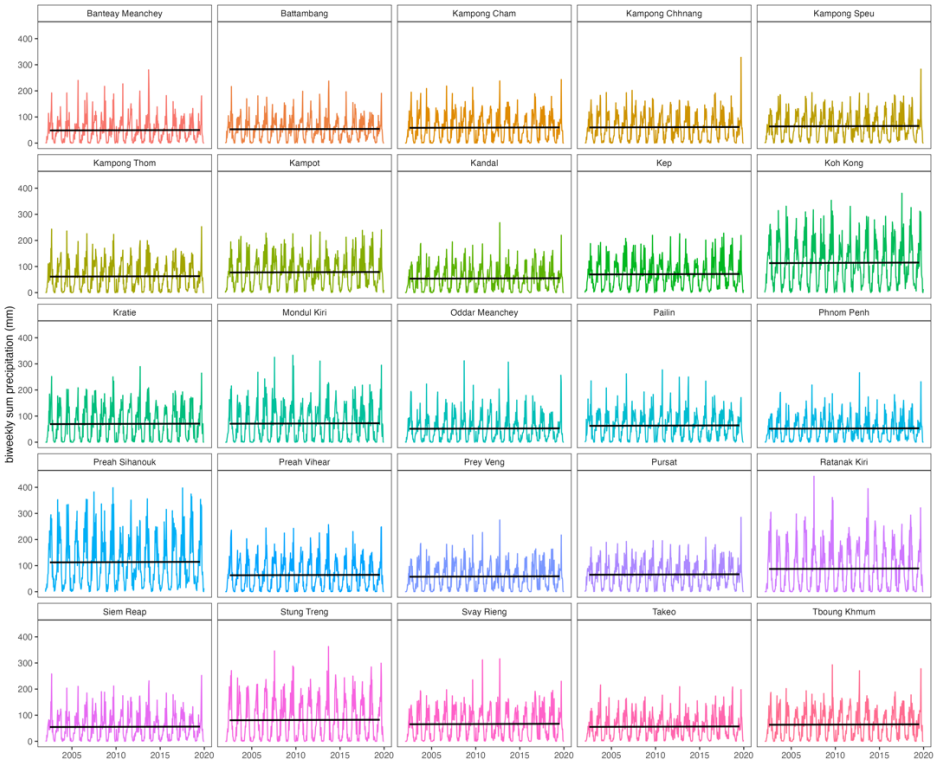

Figure S5. Identifying anomalous years in the temperature time series for Cambodia. **A** Partial effect of year, as a factor input as a smoothing spline, on response variable of mean biweekly temperature per province from GAMs (Table S1). **B** Map of Cambodia with provinces indicated by color. **C** Z-scores of temperature time series, with epidemic years indicated by vertical lines. Provinces are arranged by latitude of centroid, from south to north and colored according to map**.** The top panel gives the distribution of annual temperature z-scores across all provinces.

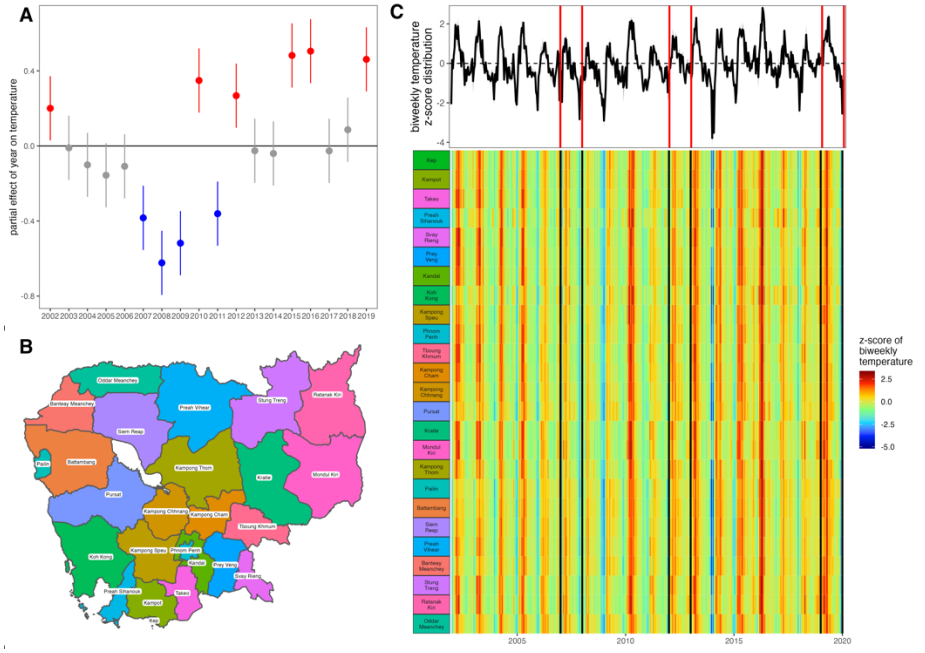

Figure S6. Identifying anomalous years in the precipitation time series for Cambodia. **A** Partial effect of year, as a factor input as a smoothing spline, on response variable of total biweekly precipitation per province from GAMs (Table S1). **B** Map of Cambodia with provinces indicated by color. **C** Z-scores of precipitation time series, with epidemic years indicated by vertical lines. Provinces are arranged by latitude of centroid, from south to north and colored according to map**.** The top panel gives the distribution of annual precipitation z-scores across all provinces.

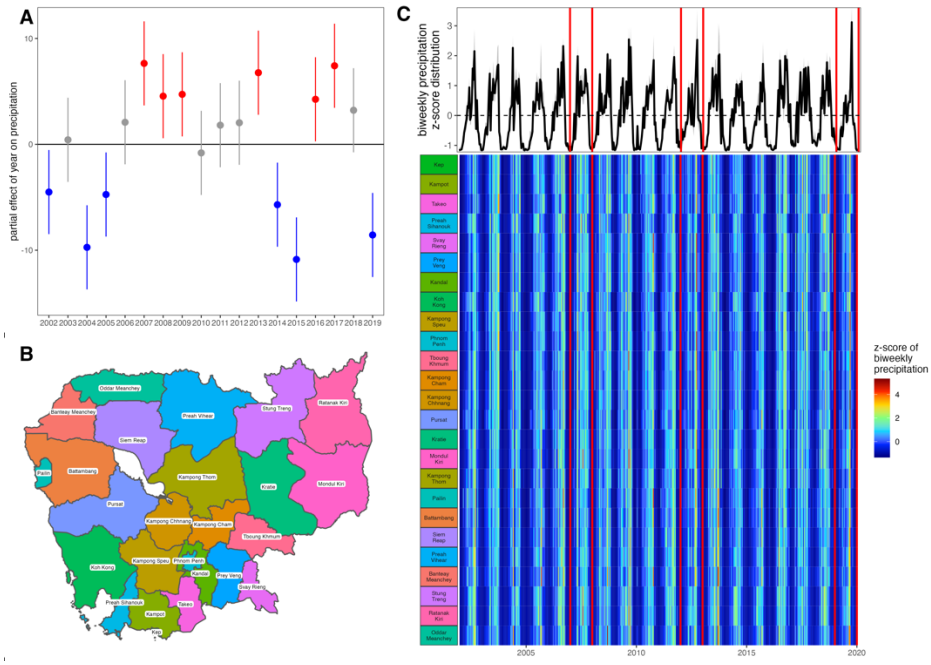

Figure S7. Impact of climate predictors on biweekly transmission rate (β) from TSIR, 2002-2006. **A** Coefficients from linear mixed effects regression, **B** coefficients from linear mixed effects regression for precipitation paired with Brière function transformation for temperature, and **C** coefficients from generalized additive model, fitted to climate variable associations with transmission rates for the 2002-2006 interepidemic period (Table S4).

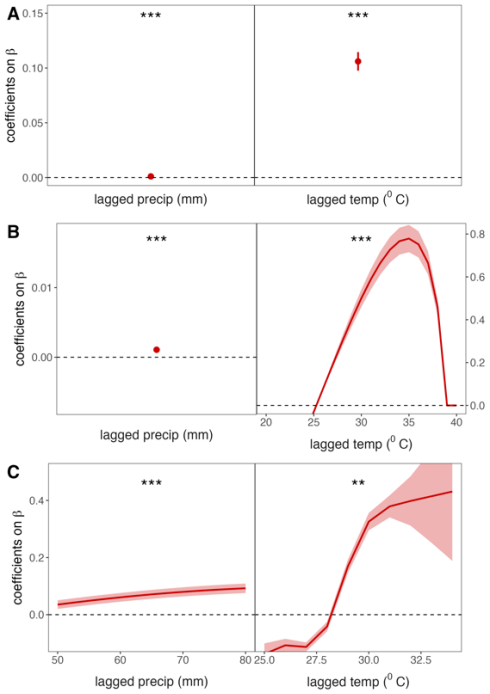

Figure S8. Impact of climate predictors on biweekly transmission rate (β) from TSIR, 2008-2011. **A** Coefficients from linear mixed effects regression, **B** coefficients from linear mixed effects regression for precipitation paired with Brière function transformation for temperature, and **C** coefficients from generalized additive model, fitted to climate variable associations with transmission rates for the 2008-2011 interepidemic period (Table S4).

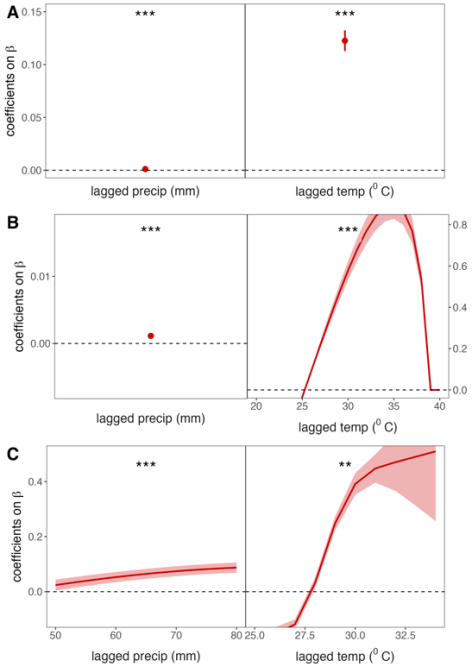

Figure S9. Impact of climate predictors on biweekly transmission rate (β) from TSIR, 2013-2018. **A** Coefficients from linear mixed effects regression, **B** coefficients from linear mixed effects regression for precipitation paired with Brière function transformation for temperature, and **C** coefficients from generalized additive model, fitted to climate variable associations with transmission rates for the 2013-2018 interepidemic period (Table S4).

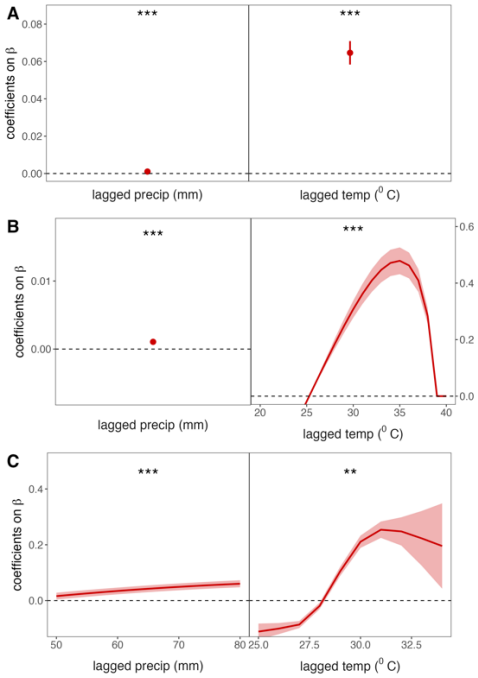

Figure S10. Biweekly dengue transmission rates, by province, from TSIR. Province-specific transmission rates (β) are colored by inter-epidemic period, according to legend, with TSIR-fitted β shown as a solid line and climate-projected β from epidemic year regressions shown as a dashed line. The 95% confidence intervals by standard error are shown in translucent shading around the mean β estimates.

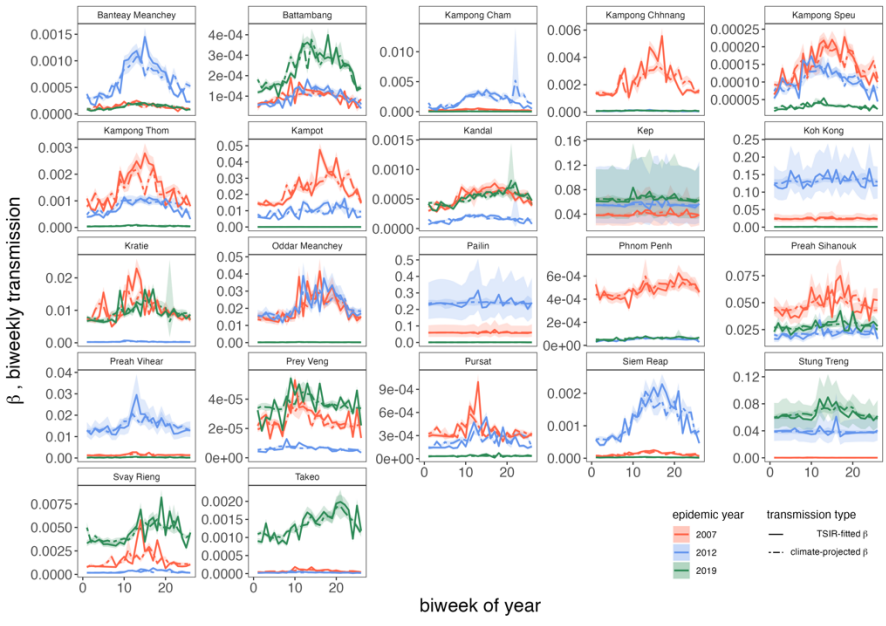

Figure S11. Average wavelet power for raw dengue incidence time series over **A** annual and **B** multiannual time horizons. **C** Proportion of provinces with which a focal province demonstrates statistically significant cross-wavelet power in the annual incidence time series or **D** between reconstructed cycles over a 5-year time horizon. Top panels give the biweekly distribution of wavelet power at annual (**A**) or multiannual (**B**) scales or the range in proportion of provinces exhibiting significant cross-wavelet power at annual (**C**) or multiannual (**D**) scales. Provinces are arranged by latitude of centroid, from south to north, colored after map in Fig. S5-S6.

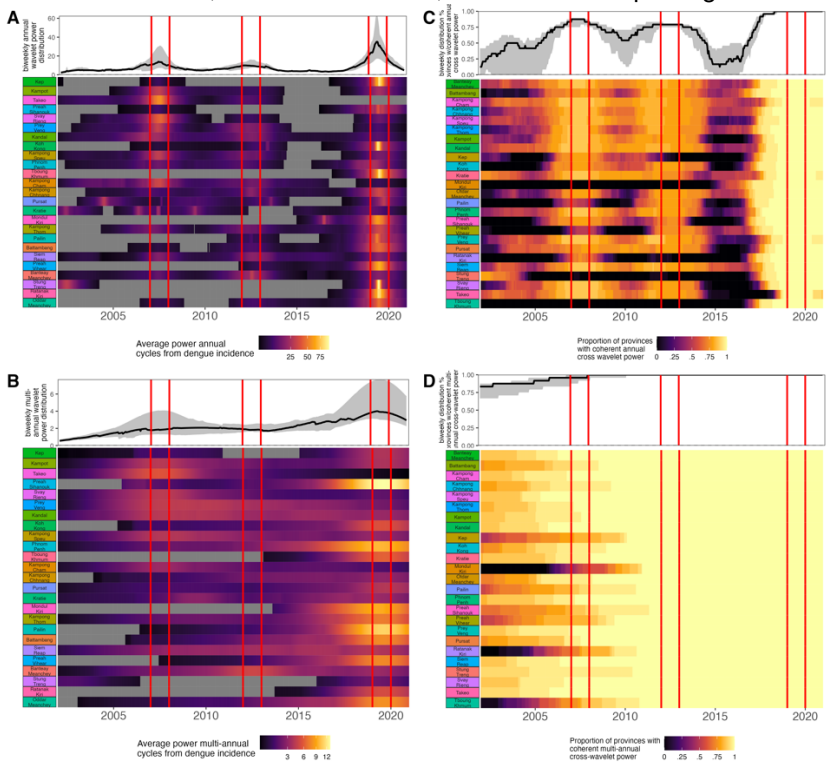

Figure S12. Predictors of annual synchronicity in annual dengue incidence between provinces. **A** Coefficient of the fixed interaction of province and geographic distance on the Pearson's correlation coefficient (ρ). **B** Partial effect of year (input as a factor), **C** mean biweekly temperature of focal province, **D** mean total annual precipitation of focal province, and **D** mean population size across the time series of focal province on ρ. Predictors with significant positive slopes are colored red, predictors with significant negative slopes colored blue, and insignificant predictors shaded gray (Table S6).

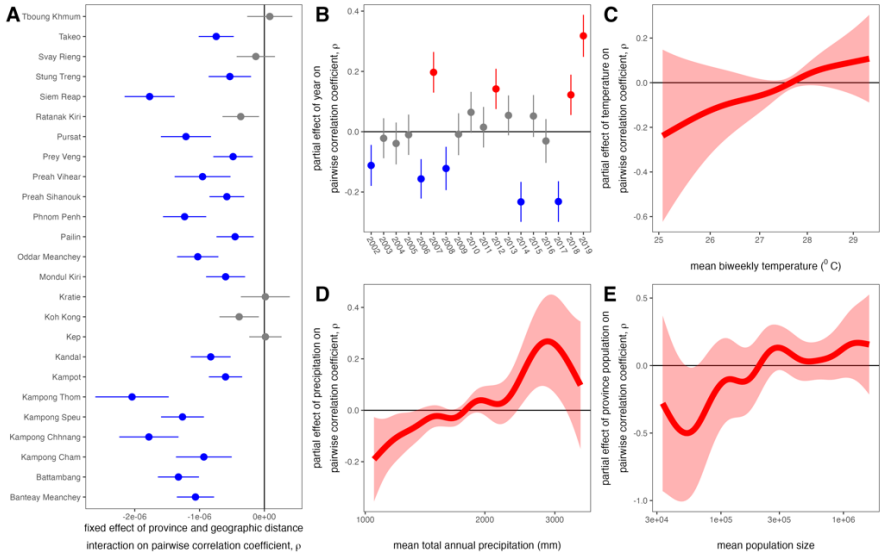

Figure S13. Cross-wavelet power between dengue dynamics and climate variables. Average cross wavelet power between biweekly raw dengue incidence and biweekly time series of **A** mean temperature and **B** total precipitation by province. Average cross-wavelet power between biweekly reconstructed multiannual dengue cycles and biweekly time series of **C** mean temperature and **D** total precipitation by province over a 5-year time horizon. **E** Average cross-wavelet power between monthly reconstructed multiannual dengue cycles and ONI by province. Top panels give the range of observed mean cross-wavelet power across all provinces. Provinces are arranged by latitude of centroid, from south to north, colored after map in Fig. S5-S6.

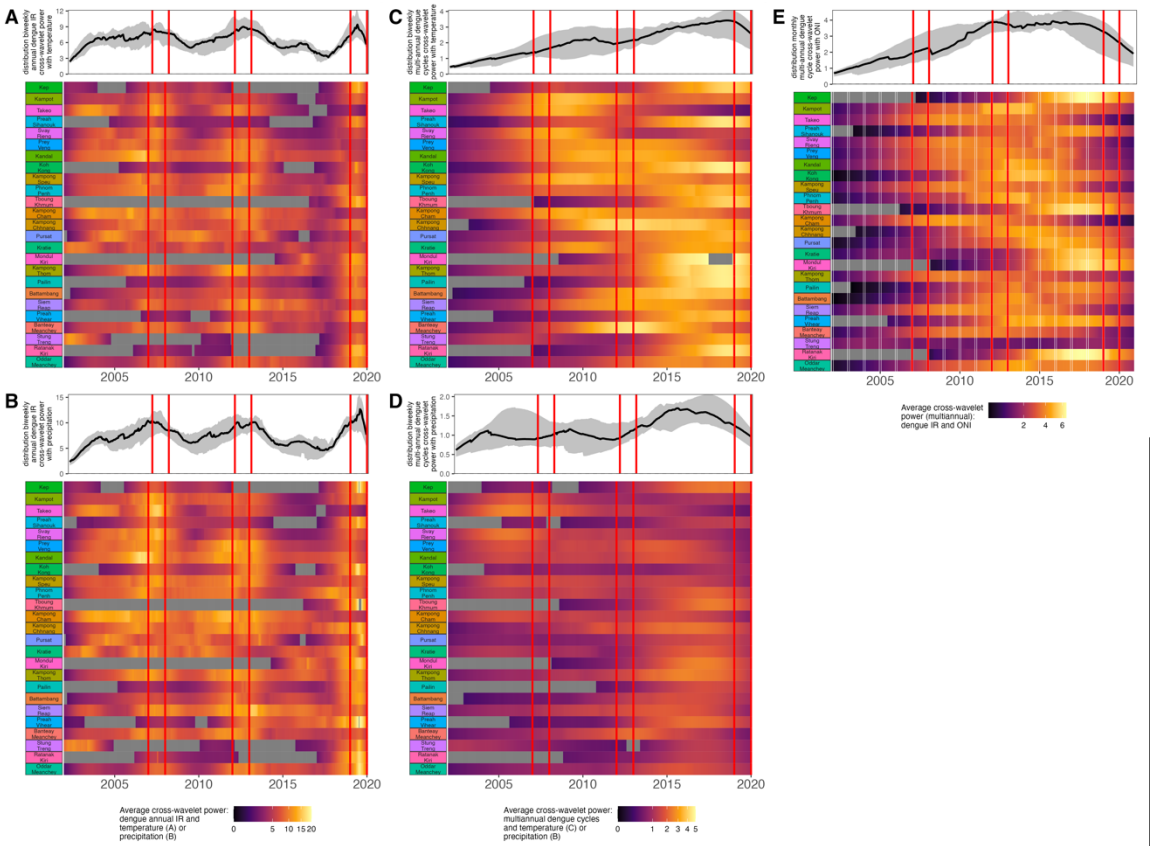

Figure S14. A Publicly available demographic data on births, deaths, and total population size preceding and overlapping the NDCP dengue time series. **B** Mean period duration of reconstructed multiannual dengue cycles for Cambodia at both national (black line) and province (colored corresponding to legend) levels across the duration of the NDCP dataset (2002-2020).

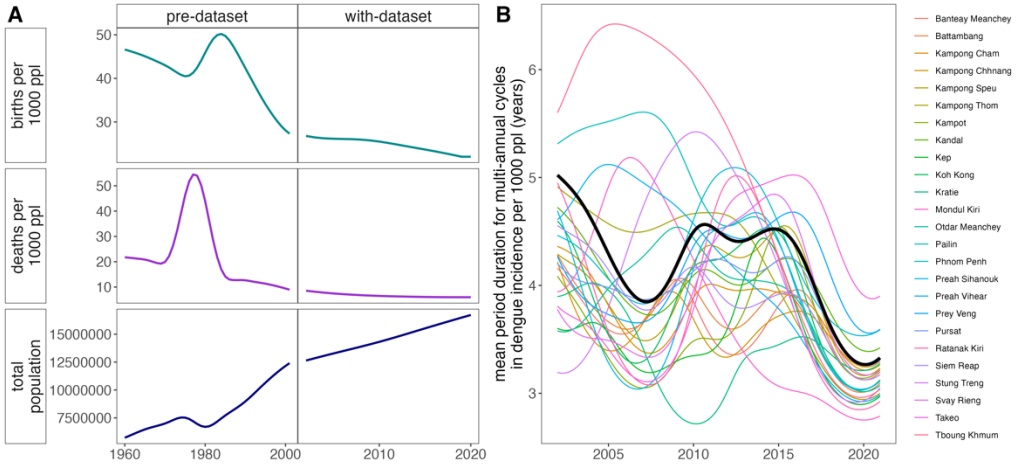

Figure S15. Age distribution of reported cases by province, with violin plots highlighting changes in the interquartile range by year. The interannual trend in the mean age of dengue infection per province is plotted as a solid black line across each province subplot, with 95% confidence intervals by standard error shown as a narrow, translucent band behind it (Table S7). Epidemic years (2007, 2012, 2019) are highlighted by dashed lines in the background.

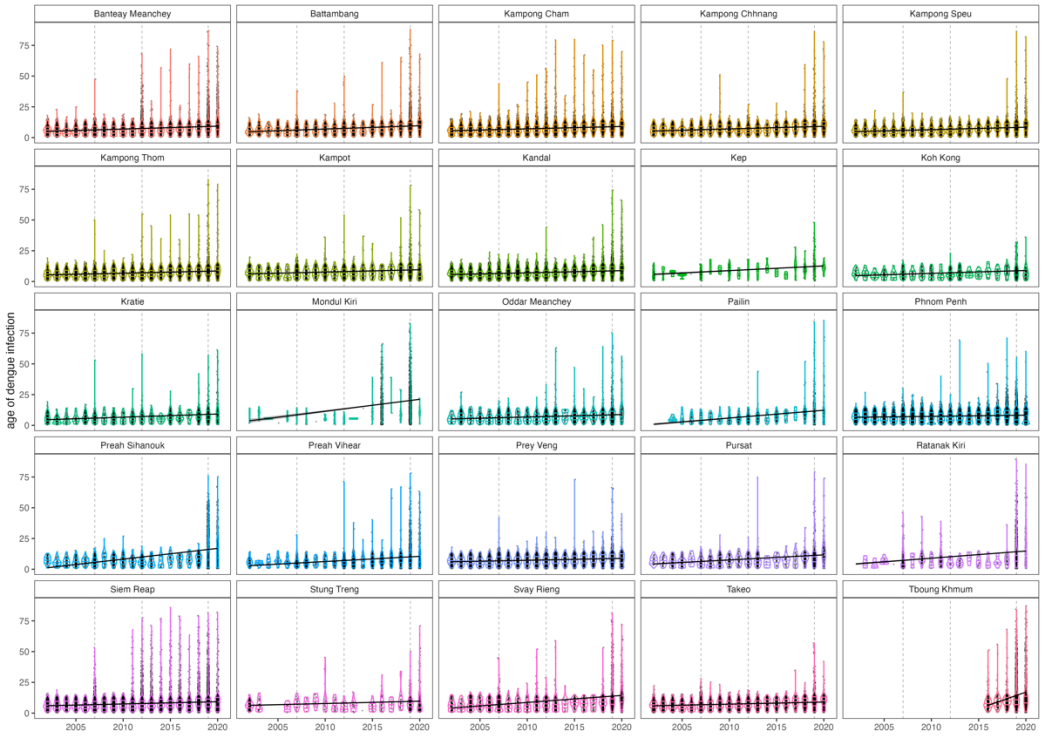

Figure S16. Annual estimates for the force of infection by year for 24 of 25 Cambodian provinces and the national time series (Tboung Khmum excluded). FOI was estimated from the birth year of the oldest individual per province, as shown collectively in Fig. 3C, using the Ferguson-Cummings catalytic model, assuming reported cases to represent secondary infections (11, 12, 20). 95% confidence intervals from the hessian matrix are shown as translucent shading.

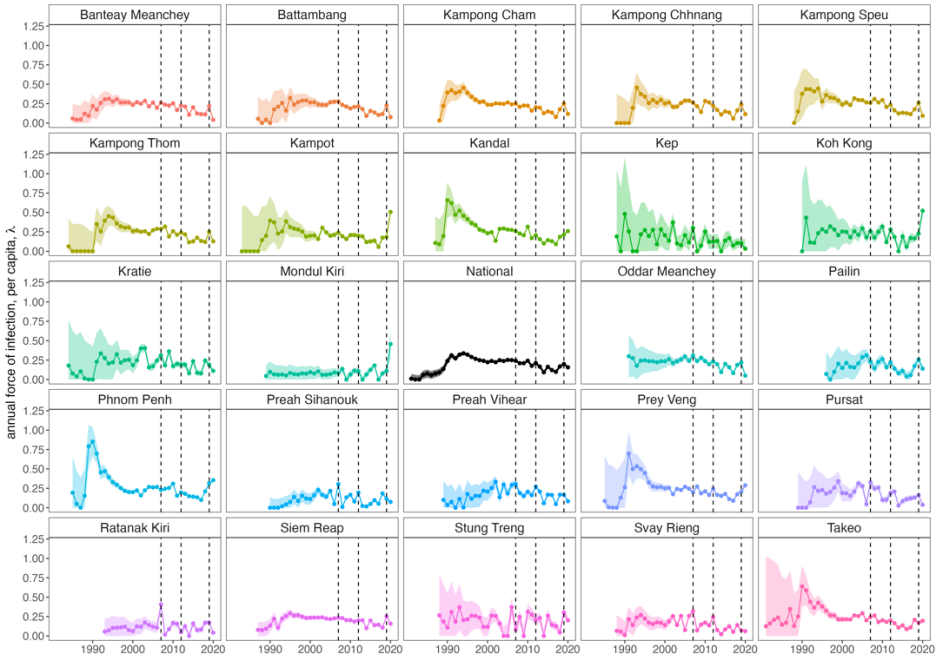

Figure S17. Cumulative proportion of cases by age by year by province, with data shown as dotted lines and model projections using FOI estimates from Fig. S16, in addition to age modification of the FOI and a rate of waning multitypic immunity in 2019 and 2020, as shown in Fig. 3D-E of the main text.

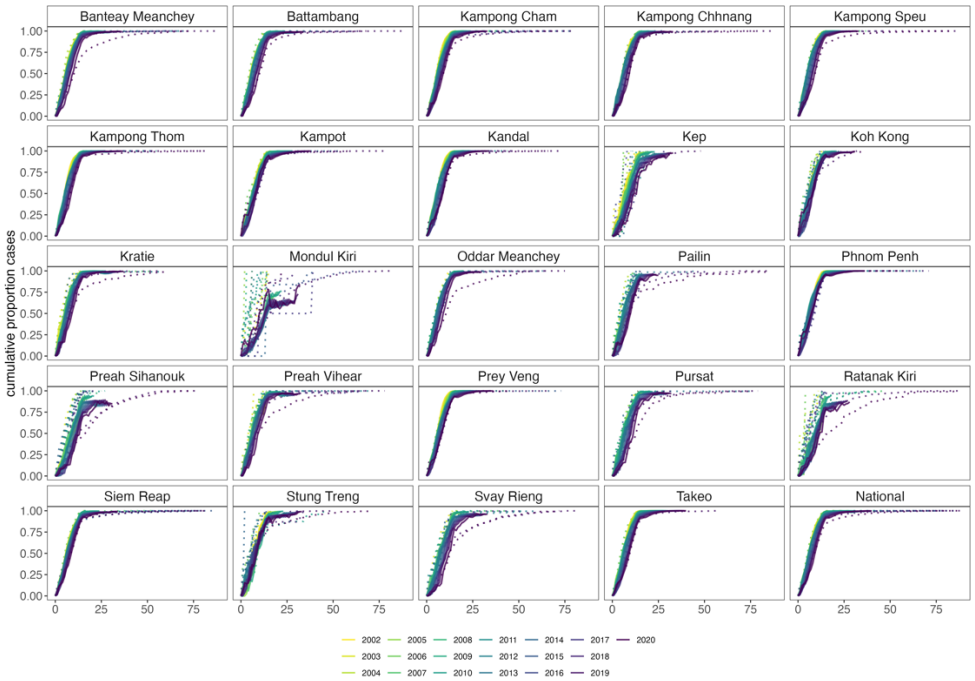

Fig. S18. Maximum likelihood phylogenetic tree constructed in RAxML (21) to illustrate how newly-contributed **A** DENV-1 and **B** DENV-2 sequences relate to all known genotypes of the corresponding serotype. Tips are colored by genotype within each serotype, with our Cambodia sequences highlighted in pink and historical Cambodia sequences available in GenBank depicted in purple. Clade bars highlight the extent of each genotype. Trees were constructed using a GTR+I+G4 nucleotide substitution model and rooted in DENV-4 (accession number NC_002640).

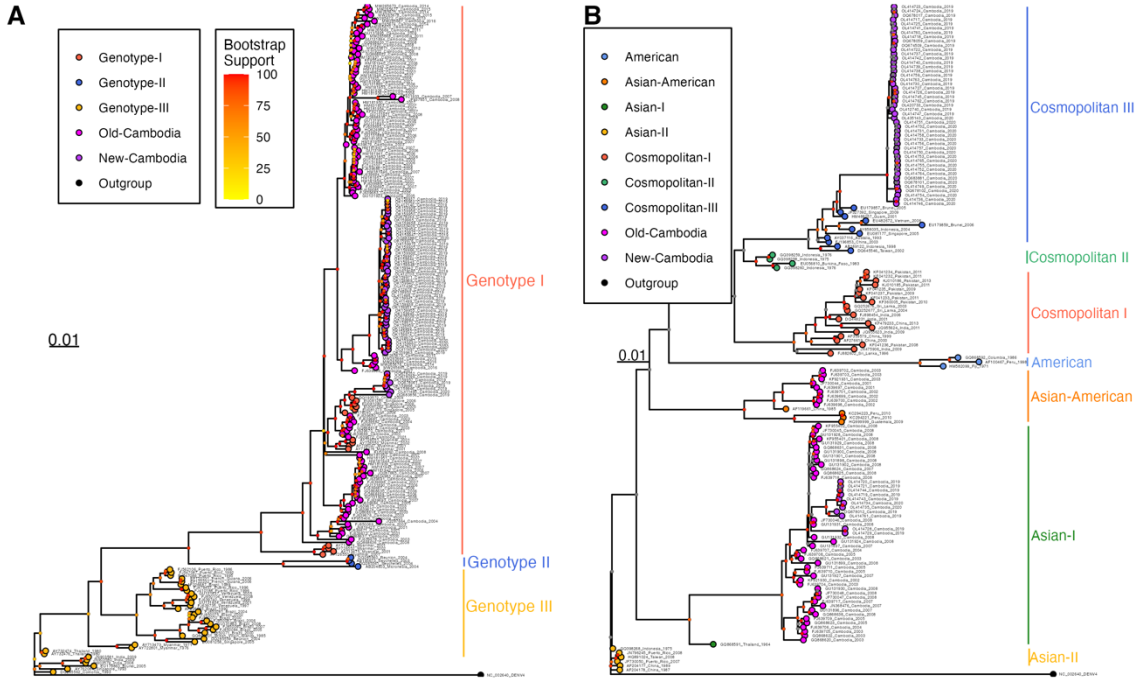

Figure S19. Geographic structuring of evolutionary relationships for DENV within Cambodia. **A** Map of Kampong Speu province, Cambodia highlighting location of all recovered sequences from our 2019-2020 active febrile surveillance. Inset detail of **B** DENV-1 and **C** DENV-2 sequences recovered from our febrile surveillance study. Tips are colored corresponding to geolocation of collection and labeled with precise date of collection and accession number.

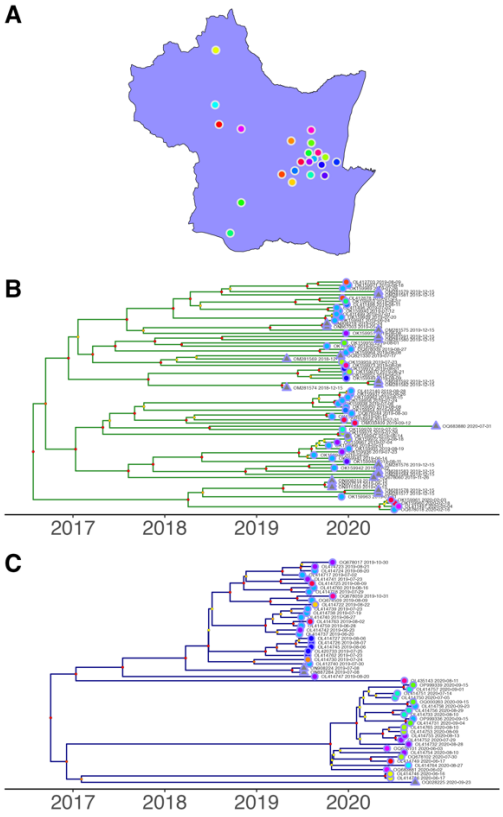

Figure S20. A Force of infection and **B** rate of waning multitypic immunity estimates recovered from fitting Ferguson-Cummings catalytic model to the age-structured time series of cases for our simulated epidemic hypotheses from Fig. 5 (main text). 95% confidence intervals from the hessian matrix are shown as translucent shading. Actual input FOI is shown in **A** as a black line. As expected, only hypotheses H2 and H3 recovered any signal of waning multitypic immunity, as witnessed in the data.

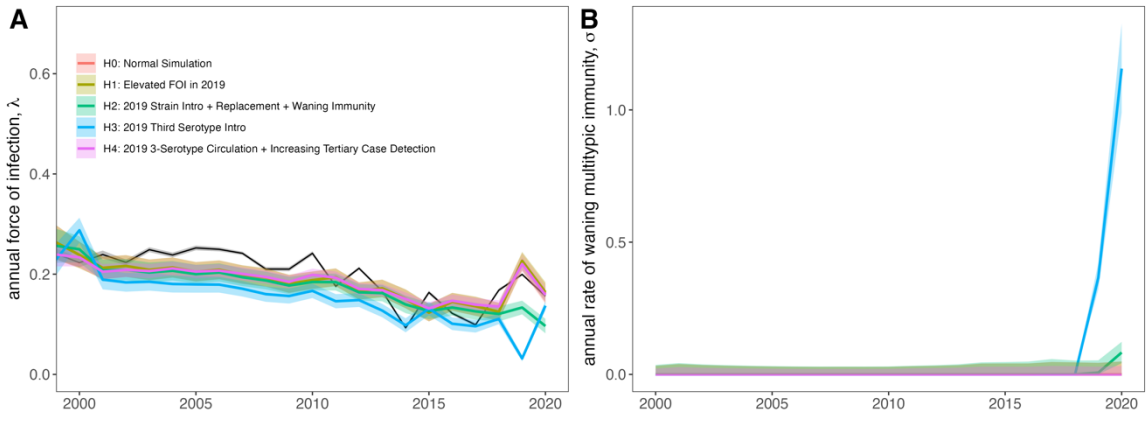

Fig S21. Simulations of hypothetical drivers of the age distribution of cases as shown in the main text (Fig. 5), here with H1, H2, and H3 perturbances introduced in 2007 instead of 2019. Panel **A** shows the mechanistic underpinnings of each simulation, **B** the total observed case counts (solid line = mean FOI; translucent shading = 95% confidence interval for FOI), **C** the age distribution of cases by year (secondary = black; tertiary = blue), and **D** the cumulative proportion of cases by age through time.

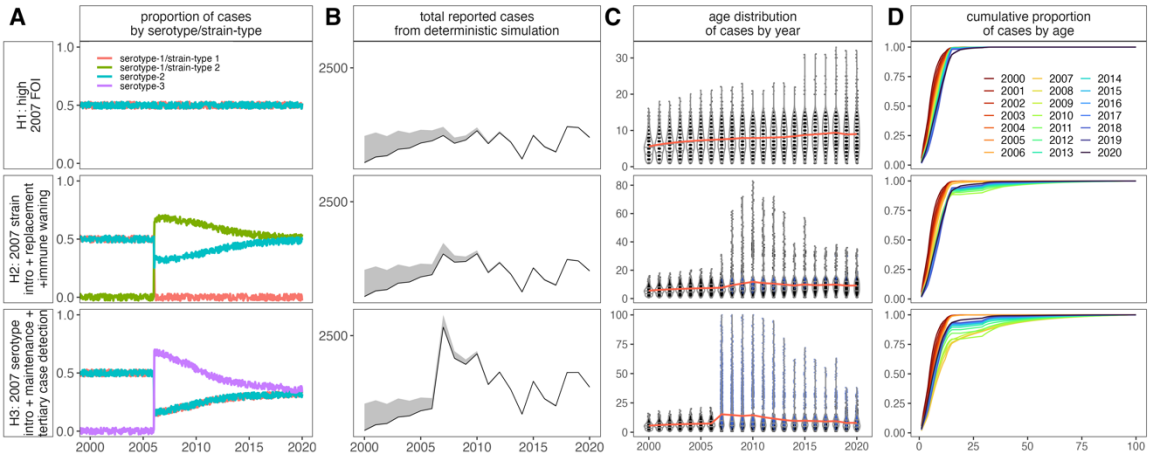

Supplementary Tables

All supplementary tables have been stored in Supplementary Dataset 1, accompanying the main text of the paper. We here provide a brief bibliography of the tables listed:

Table Number	Table Title
Table S1	Generalized additive model summaries for climate data
Table S2	Fitted TSIR parameters by province
Table S3	Optimal climate lags to predict biweekly transmission, by inter-epidemic period and province
Table S4	Summary of regression models relating lagged temperature and precipitation to transmission
Table S5	Fraction of increased susceptibles needed to recapture epidemic year caseloads, with and without climate-informed transmission rate
Table S6	Generalized additive model summary for predictors of synchronicity
Table S7	Generalized additive model summary for age of dengue infection
Table S8	FOI fits and model selection with age modifiers and waning multitypic immunity
Table S9	GenBank accession numbers of DENV genomes added in part with this study

SI References

1. W. O. Kermack, A. G. McKendrick, Contributions to the mathematical theory of epidemics II: The problem of endemicity. *Proceedings of the Royal Society A* **115**, 55–83 (1932).

2. R. M. Anderson, R. M. May, *Infectious Diseases of Humans: Dynamics and Control* (Oxford University Press, 1991).

3. A. D. Becker, B. T. Grenfell, TSIR: An R package for time-series susceptible-infected-recovered models of epidemics. *PLoS ONE* **12**, 1–10 (2017).

4. B. T. Grenfell, O. N. Bjornstad, B. F. Finkenstadt, Dynamics of measles epidemics: Scaling noise, determinism, and predictability with the TSIR Model. *Ecological Monographs* **72**, 185–202 (2002).

5. B. F. Finkenstadt, B. T. Grenfell, T. Grenfell, Time series modelling of childhood diseases: a dynamical systems approach. *Journal of the Royal Statistical Society, Series C (Applied Statistics)* **49**, 187–205 (2000).

6. O. N. Bjornstad, B. F. Finkenstadt, B. T. Grenfell, Dynamics of measles epidemics: Estimating scaling of transmission rates using a times series SIR model. *Ecological Monographs* **72**, 169–184 (2002).

7. S. N. Wood, mgcv: GAMs and Generalized Ridge Regression for R. *R News* **1/2**, 20–24 (2001).

8. C. E. Wagner, *et al.*, Climatological, virological and sociological drivers of current and projected dengue fever outbreak dynamics in Sri Lanka. *Journal of the Royal Society Interface* **17** (2020).

9. M. U. G. Kraemer, *et al.*, Big city, small world: density, contact rates, and transmission of dengue across Pakistan. *J. R. Soc. Interface.* **12**, 20150468 (2015).

10. L. C. Katzelnick, *et al.*, Antigenic evolution of dengue viruses over 20 years. *Science* (2021).

11. N. M. Ferguson, C. A. Donnelly, R. M. Anderson, Transmission dynamics and epidemiology of dengue: insights from age-stratied sero-prevalence surveys. *Proceedings of the Royal Society B* **354**, 757–768 (1999).

12. D. A. T. Cummings, *et al.*, The impact of the demographic transition on dengue in Thailand: Insights from a statistical analysis and mathematical modeling. *PLoS Medicine* **6** (2009).

13. P. Klepac, *et al.*, Stage-structured transmission of phocine distemper virus in the Dutch 2002 outbreak. *Proceedings. Biological sciences / The Royal Society* **276**, 2469–2476 (2009).

14. P. Klepac, H. Caswell, The stage-structured epidemic: Linking disease and demography with a multi-state matrix approach model. *Theoretical Ecology* **4**, 301–319 (2011).

15. C. J. E. Metcalf, *et al.*, Structured models of infectious disease: Inference with discrete data. *Theoretical Population Biology* **82**, 275–282 (2012).

16. United Nations, United Nations Department of Economic and Social Affairs: Population by Age Groups–Both Sexes. (2022).

17. World Bank, Cambodia. *World Development Indicators* (2021) (April 12, 2022).

18. United Nations, United Nations Department of Economic and Social Affairs: Deaths by Single Age - Both Sexes. (2022).

19. N. G. Reich, *et al.*, Interactions between serotypes of dengue highlight epidemiological impact of cross-immunity. *J. R. Soc. Interface.* **10**, 20130414 (2013).

20. Hugo. Muench, *Catalytic models in epidemiology.* (Harvard University Press, 1959).

21. A. M. Kozlov, D. Darriba, T. Flouri, B. Morel, A. Stamatakis, RAxML-NG: A fast, scalable and user-friendly tool for maximum likelihood phylogenetic inference. *Bioinformatics* **35**, 4453–4455 (2019).